HHS Public Access

Author manuscript

Ann Biomed Eng. Author manuscript; available in PMC 2017 April 01.

Published in final edited form as:

Ann Biomed Eng. 2016 April ; 44(4): 1019–1035. doi:10.1007/s10439-015-1370-z.

Hemodynamics in a Pediatric Ascending Aorta Using a Viscoelastic Pediatric Blood Model

Bryan C. Good[1], **Steven Deutsch**[1], and **Keefe B. Manning**[1,2]

[1]Department of Biomedical Engineering, The Pennsylvania State University, 205 Hallowell Building, University Park, PA 16802, USA

[2]Department of Surgery, Penn State Hershey Medical Center, Hershey, PA 17033, USA

Abstract

Congenital heart disease is the leading cause of infant death in the United States with over 36,000 newborns affected each year. Despite this growing problem there are few mechanical circulatory support devices designed specifically for pediatric and neonate patients. Previous research has been done investigating pediatric ventricular assist devices (PVADs) assuming blood to be a Newtonian fluid in computational fluid dynamics (CFD) simulations, ignoring its viscoelastic and shear-thinning properties. In contrast to adult VADs, PVADs may be more susceptible to hemolysis and thrombosis due to altered flow into the aorta, and therefore, a more accurate blood model should be used. A CFD solver that incorporates a modified Oldroyd-B model designed specifically for pediatric blood is used to investigate important hemodynamic parameters in a pediatric aortic model under pulsatile flow conditions. These results are compared to Newtonian blood simulations at three physiological pediatric hematocrits. Minor differences are seen in both velocity and WSS during early stages of the cardiac systole between the Newtonian and viscoelastic models. During diastole, significant differences are seen in the velocities in the descending aorta (up to 12%) and in the aortic branches (up to 30%) between the two models. Additionally, peak wall shear stress (WSS) differences are seen between the models throughout the cardiac cycle. At the onset of diastole, peak WSS differences of 43% are seen between the Newtonian and viscoelastic model and between the 20 and 60% hematocrit viscoelastic models at peak systole of 41%.

Key terms

Oldroyd-B; computational fluid dynamics; wall shear stress; viscoelasticity

Correspondence: Keefe B. Manning, Ph. D., Department of Bioengineering, The Pennsylvania State University, 205 Hallowell Building, University Park, PA 16802, USA, Phone: 1-814-863-6318, Fax: 1-814-863-0490, kbm10@psu.edu.

There are no conflicts of interest.

Disclosures

The authors have no disclosures.

Introduction

Each year between 1500–2000 infants and children are added to the heart transplantation list with approximately 350 successfully receiving transplants[5]. These patients face the highest wait-list mortality in transplantation medicine, with 23% of infants (<12 months) dying within six months of being added[25]. Historically, extracorporeal life support (ECMO) has been used as a bridge to transplant for these patients and occasionally adult ventricular assist devices (VADs) have been used in older children. Only recently has a pediatric ventricular assist device (PVAD), the Berlin Heart EXCOR, been approved for use in the United States as a bridge to transplantation for children of various sizes[1]. However, compared to adult patients, infants and children have few reliable devices designed specifically for them. In 2004, the US government through the National, Heart, Lung, and Blood Institute awarded contracts to five groups to develop pediatric mechanical circulatory support devices[4]. As part of developing a reliable pediatric ventricular assist device (PVAD), it is necessary to accurately predict the hemodynamics because of the higher hemolysis and thrombosis rates resulting from PVADs compared to adult LVADs[3].

Previous experimental and computational fluid dynamics (CFD) studies have been completed on human adult aorta models looking at hemodynamics in the aortic arch and descending aorta. Chandran showed with flow visualization techniques that blood flow skewed toward the inner wall of curvature during systole, velocity profiles remained relatively flat throughout the model and the flow did not fully develop by the time it reached the descending aorta[6]. Shahcheraghi *et al.*, showed similar results with CFD; that inlet flow is skewed toward the inner aortic wall, flow downstream of the branches is skewed toward the outer wall, and flow within the branches is skewed toward the distal walls[34]. Additional work has been completed on pediatric cardiovascular models with cardio-pulmonary bypass[29], Fontan circulation[30], and end-to-side anastomosis[37,38], comparing healthy, diseased and surgically repaired pediatric aortic flows. All of these studies have been performed with the assumption that blood behaves as a Newtonian fluid.

It is known, however, that blood is a viscoelastic fluid with a non-uniform viscosity and elasticity that varies with shear rate. At high shear rates (>500 s^{-1}) blood viscosity remains constant due to its red blood cells (RBCs) aligning in layers with the direction of flow. At low shear rates (<100 s^{-1}) blood viscosity and elasticity increase exponentially with decreasing shear rate due to the aggregation of RBCs and storage of elastic energy[7,8]. Thurston first proposed an extended Maxwell model (a viscous damper and elastic spring in series) for blood, but later realized a critical shear rate beyond which assumptions of linear viscoelasticity and Newtonian behavior of blood ceased to hold[35]. Oldroyd-B type models for blood have been developed by Phillips and Deutsch[31] and Yeleswarapu[40] but their model relaxation times are not shear rate dependent. A Generalized Oldroyd-B (GOB) model has been developed by Rajagopal and Srinivasa[32] that more accurately models blood by incorporating four independent parameters that reflect the elasticity, plasma viscosity, RBC aggregation and its effect on viscosity, and shear-thinning that occurs during flow. A complication of Oldroyd-B type models is that they have an unbounded extensional viscosity that can lead to an over prediction of stress[9]. To address this, models such as Giesekus and

Leonov include an additional term to bound the polymeric stress component related to the particular physical model[13,21].

Pediatric blood, as compared to adult blood, has much lower plasma viscosity and decreased RBC aggregation at low shear rates due to decreased plasma protein concentration (primarily fibrinogen)[22,33]. Therefore, any pediatric viscoelasticity model must accurately capture these high and low shear rate differences. Long *et al.*, using previously collected pediatric viscosity and elasticity data, developed non-linear regression equations for viscosity as a function of both patient hematocrit and shear rate[24].

The purpose of this study is to investigate the effect of pediatric blood viscoelasticity on hemodynamics in a pediatric ascending aorta using modified Oldroyd-B constitutive equations specifically developed for pediatric blood. Velocity and wall shear stress (WSS) are analyzed and compared between Newtonian and Generalized Oldroyd-B (GOB) blood models at three different physiological pediatric hematocrits.

Methods

Geometric Model

Hemodynamic parameters are dependent on the local geometry of the aorta, and therefore, a pediatric patient's aorta (8 years old) is used. The model is reconstructed using magnetic resonance imaging (MRI, NIH-Georgia Tech Fontan Anatomy Database ID: CHOP007) and scaled down to represent a one year old pediatric patient with an aortic inlet diameter of 11.6 mm. All of the dimensions of the aortic model are within the range of morphological measurements previously reported by Machii and Becker[25]. Each branch vessel is extended ten times its diameter to allow the branch inlet flows to be independent of the outlet boundary conditions (Fig. 1A).

Viscoelastic Model

To fully capture the viscoelastic and shear-thinning properties of human blood, a generalized Oldroyd-B (GOB) model developed by Rajagopal and Srinivasa is modified for pediatric blood[32]. The GOB model, based on a thermodynamic framework for non-linear rate type fluids, uses both the continuity equation (Eq.1) and momentum equation (Eq.2), splitting the stress tensor into a solvent component (representing blood plasma) (Eq.3) and a polymeric component (representing RBCs).

$$\nabla \cdot \underline{u} = 0 \quad \text{(Eq. 1)}$$

$$\rho \frac{\partial \underline{u}}{\partial t} + \rho \underline{u} \cdot \nabla \underline{u} = -\nabla p + \nabla \cdot (\tau_s + \tau_p) \quad \text{(Eq. 2)}$$

$$\tau_s = 2\eta_\infty D \quad \text{(Eq. 3)}$$

Where $\underline{u}$ is the fluid velocity vector, ρ is the fluid density, p is the pressure, τ is the total stress tensor composed of both the solvent (τ_s) and polymeric (τ_p) parts, η_∞ is the solvent viscosity, and D is the symmetric part of the velocity gradient.

The polymeric stress component is modeled by Rajagopal and Srinivasa with a neo-Hookean elastic response and a dissipative response that is quadratic in the stretch tensor with an added term mimicking that for a Newtonian fluid (Eq.4 and Eq.5).

$$\tau_p+\frac{\eta}{2\mu}\check{\tau}_p=\mu\lambda I \quad \text{(Eq. 4)}$$

$$\lambda=\frac{3}{tr(B^{-1})} \quad \text{(Eq. 5)}$$

Where η is the solvent viscosity, μ is the elastic shear modulus, λ is the relaxation time, B is the left Cauchy stretch tensor and $\check{\tau}_p$ is the upper-convected time derivative (or Oldroyd derivative) of the polymeric stress. As previously discussed, Oldroyd-B type models can be very accurate in simple shear flow cases but in extensional flows, like the curved pipe flow in an aorta, they can over predict the polymeric stresses due to an unbounded stretching of the linear spring element in the model. The Giesekus and Leonov models have been developed with a non-linear physiological "drag force" included to bound the equation. The Giesekus model includes a 'mobility' parameter (α) that can vary between 0 and 0.5 while the Leonov model uses a fixed value of 0.5[13,21]. Previous research using the Giesekus model for pony blood found that for a hematocrit of 37% the mobility parameter was 0.489[16]. For this reason, a Giesekus/Leonov-like term will be added to the GOB model with a constant α value of 0.5 (Eq. 6).

$$\tau_p+\frac{\eta}{2\mu}\check{\tau}_p+\alpha\frac{2\mu}{\eta}(\tau_p\cdot\tau_p)=\mu\lambda I \quad \text{(Eq. 6)}$$

Boundary Conditions

A scaled plug flow velocity waveform (cardiac output of 1 L/min and heart rate of 120 bpm) acquired from an *in vivo* study of PVAD function in infant animal models[28] (Fig. 1B) is applied at the inlet of the ascending aorta to mimic a healthy pediatric patient. The outlets of the three aortic branches and of the aortic arch are given resistance boundary conditions for pressure to achieve physiological flow splitting:

$$p=RQ+p_0 \quad \text{(Eq. 7)}$$

Where p is the pressure, Q is the flow rate, R is a resistance constant and p_0 is the aortic outlet pressure (assumed to be 60 mmHg[19]). For pediatric patients, 40–50% of cardiac output is diverted from the aortic arch into the branch vessels and flow in each respective branch vessel is proportional to its cross-sectional area[19]. Numerical studies were performed

to determine the correct resistance constant (R) at each outlet such that the total flow splitting into the vessels is 46.75%; 21.41%, 10.58% and 14.76% into the brachiocephalic, left common carotid and left subclavian arteries, respectively[38]. The resistance constants were found to be $2.4e^4$, $2.4e^5$, $3.6e^5$, and $1.8e^5$ Pa·s/m^3 for the brachiocephalic artery, left common carotid artery, left subclavian artery and the aortic outlet, respectively, and were maintained for each simulation. Additionally, zero velocity gradient boundary conditions were applied at all outlets and no slip boundary conditions on all walls.

Grid Generation

High-quality unstructured grids have been generated using GAMBIT 2.3.16 (Fluent Inc., Lebanon, NH). Three grids (coarse ~ 180,000 cells; medium ~ 580,000 cells; and fine ~ 1,600,000 cells) were constructed for a systematic grid study. The heights of near-wall cells are approximately 0.5, 0.1, and 0.05 mm, respectively. The interior cells are a mixture of tetrahedral and hexahedral grids with nearly isotropic sizes of 1.0, 0.7, and 0.5 mm, respectively.

Flow Solver

OpenFOAM (OpenCFD Ltd), a C^{++} open-source CFD software that allows for user customized numerical solvers and pre and post-processing utilities, is used in this study. A previously validated OpenFOAM solver for viscoelastic fluids developed by Favero *et al.*[10], viscoelasticFluidFoam, is used to solve the system of viscoelastic equations (Eqs. 1–6). In brief, viscoelasticFluidFoam takes the initial given fields and explicitly calculates the pressure gradient and stress divergence. Next, the momentum equation is implicitly solved for a new velocity field. The new velocity values are used to estimate a new pressure field and corrected using the pressure-implicit splitting operators (PISO)[17] scheme to satisfy continuity. Finally, a new stress tensor field is calculated using the chosen constitutive equation. For transient flows, this algorithm is iterated at each time step to achieve a desired accuracy.

The governing and constitutive equations are discretized using a finite volume method. The linear solvers used are a generalized geometric/algebraic multi-grid (GAMG) solver for pressure and a preconditioned bi-conjugate gradient (PBICG) solver for the velocity and stress tensors. A dynamic time-step control is used to maintain the Courant number under 1 throughout the entire cardiac cycle and the residuals of all variables are converged to 10^{-6} at every time step.

Pediatric Viscosity Data

Viscosity versus shear rate data were used based on previously published data[24] from pediatric patients (4 days to 7.7 years). From the developed non-linear regression equations, viscosity versus shear rate curves were generated for pediatric blood hematocrits of 20, 40 and 60%, representing the potential hematocrit ranges in neonates and pediatric patients (Fig. 2).

Results

Fit of Pediatric Viscosity Data

The modified GOB model coefficients (Table 1) were found from the pediatric viscosity versus shear rate data and an apparent viscosity model corresponding to the chosen GOB model[2]. η and η_1 are functions of the asymptotic viscosities corresponding to zero (η_0) and infinite (η_∞) shear rates and were found directly from the data at shear rates of 0.1 and 200 s^{-1}, respectively (Eqs. 8–9).

$$\eta = 2(\eta_0 - \eta_\infty) \quad \text{(Eq. 8)}$$

$$\eta_1 = 2\eta_\infty \quad \text{(Eq. 9)}$$

The elastic shear modulus (μ) was determined using a least squares fit of Eqs. 10 and 11 to the pediatric viscosity versus shear rate data (Fig. 2)

$$\mu_{exp} = \frac{\eta\lambda + \eta_1}{2} \quad \text{(Eq. 10)}$$

$$\lambda = \frac{1}{\left[1 + \frac{1}{\left(\frac{\eta\dot{\gamma}}{2\mu}\right)^2}\right]^{1/3}} \quad \text{(Eq. 11)}$$

Where μ_{exp} is the experimental viscosity and $\dot{\gamma}$ is the experimental shear rate. The fit of the GOB model shows excellent agreement with the pediatric viscosity data for all three hematocrits. The infinite-shear rate viscosity for these models was assumed to be the viscosity at the highest shear rate measured in the data set[20]. However, for the 60% hematocrit, the apparent viscosity model at 200 s^{-1} is still slightly converging to its true asymptotic infinite-shear rate viscosity leading to a very small over prediction of the η_1 parameter (< 2%)

Solver Validation

The solver itself, viscoelasticFluidFoam, has previously been validated by Favero *et al.*[10] for several viscoelastic models. To validate this particular modified GOB model a 4:1 planar contraction test geometry (Fig. 3A) with an upstream thickness of 0.0254 m and a downstream thickness of 0.0064 m was used with a constant inlet flow rate of 250 cm^3/s to compare results between a previously validated Giesekus model[13] fit to the same fluid data coefficients. Three horizontal and three vertical velocity profiles were analyzed upstream of the contraction and three vertical velocity profiles were analyzed downstream of the contraction as done in previous validation studies[10]. Excellent agreement was seen between the GOB and Giesekus models' velocity profiles. The largest differences were seen in the horizontal plane 'A' right near the top corner of the model where the GOB model slightly over predicts the velocity magnitude compared to the Giesekus model by approximately 6%

(Fig. 3B). Additional minor discrepancies exist in Figure 3C near the wall where at both planes 'F' and 'E' the GOB model over predicts the velocity by less than 5%. At very other point in the flow there is excellent agreement between the GOB model and the previously validate Giesekus model.

Grid Sensitivity Analysis

A systematic grid study is performed to verify the numerical solutions. The pressures and volumetric flow rates at the inlet and outlets of the pediatric aortic model are measured throughout a full cardiac cycle. Figure 4 shows the pressure waveforms integrated over each inlet and outlet patch as a function of time. Only minor differences are seen during the flow reversal phase for the coarse grid in Figs. 4C and 4D. No significant differences are observed at any patch or time point between the medium and fine grids. Similar results were seen comparing the volumetric flow rates at the inlet and outlets with no differences seen between the medium and fine grids and are thus not included. The systolic and diastolic pressures are 99 and 60 mmHg, respectively, measured at the inlet of the aorta, and are well within physiological parameters for a 1 year old patient[19].

Figure 5 shows the effect of grid refinement on WSS at six locations along the length of the aortic wall. WSS is more sensitive to the grid compared to flow rate and pressure. Different WSS results are seen during peak systole for the coarse grid compared to the medium and fine grids. However, excellent agreement is seen between the medium and fine grids throughout the cardiac cycle with the largest differences seen at peak systole in locations 3, 4, and 6. These differences were approximately 4, 6 and 3%, respectively. For these reasons, the medium grid is used for the remainder of the simulations.

Comparison of Newtonian and GOB blood models

The modified GOB model is compared to a Newtonian model to determine the differences that come from more accurately modeling blood's viscoelastic properties. The Newtonian model was given a dynamic viscosity that matched the infinite shear rate viscosity of the corresponding hematocrit GOB model. The viscosity values were 2.9, 4.5 and 7.4 centipoise for the 20, 40 and 60% hematocrits, respectively. Figure 6 shows velocity magnitude contours for both the 60% hematocrit Newtonian and GOB blood models at three different points in the cardiac cycle (peak systole, mid-deceleration of systole and onset of diastole). At peak systole the two models predict nearly the same flow field with maximum velocities seen in the descending aorta of 1.36 m/s, in the ascending aorta of 1.21 m/s and in the left subclavian artery of 1.34 m/s. At mid-deceleration of systole, the two models again are very similar but with slight differences in the peak velocities seen in the descending aorta, outer wall of the aortic arch and the left subclavian artery. In the GOB model these velocities were 0.98 m/s, 0.84 m/s, and 0.68 m/s, respectively while the velocities in the same locations in the Newtonian model were 2–3% higher. In both models at these early systolic time points the flow profile is skewed toward the inner wall as it enters the aortic arch and moves toward the outer wall as it passes through the aortic arch and into the descending aorta. Later in the cardiac cycle at the onset of diastole there are major differences in the velocity fields. The flow is skewed much more towards the outer wall of curvature in the aortic arch and into the aortic branches in the Newtonian model while flow remains more in the center of the aorta

with the GOB model. Peak velocities are higher in the GOB than the Newtonian model in the descending aorta (0.4 m/s compared to 0.35 m/s) but are lower in the ascending aorta (0.15 m/s compared to 0.24 m/s) and in both the brachiocephalic and left subclavian arteries (0.27 m/s compared to 0.39 m/s).

WSS values were also compared between the 60% hematocrit Newtonian and GOB models at four different points in the cardiac cycle (peak systole, mid-deceleration of systole, onset of diastole, and mid-diastole) (Figure 7). At peak systole, the WSS values between the two models are similar but with the GOB model predicting higher stresses between the left subclavian and left common carotid arteries (931 vs. 915 dyne/cm^2) and between the left common carotid and brachiocephalic arteries (912 vs 880 dyne/cm^2). During mid-deceleration of systole again the GOB model predicts a peak WSS value of 425 dyne/cm^2 compared to 403 dyne/cm^2 in the Newtonian model. At the two later time points in the cardiac cycle, however, the Newtonian model predicts distinctly higher WSS values than the GOB model. At the onset of diastole, the Newtonian model shows peak WSS values of approximately 115 dyne/cm^2 at the branches of the left subclavian and left common carotid arteries compared to only 65 dyne/cm^2 in the GOB model. Additionally, WSS values along the distal wall of the ascending aorta and proximal wall of the descending aorta are on average 10–15 dyne/cm^2 higher in the Newtonian model. Midway through diastole, WSS values have decreased significantly in the GOB model and are mostly uniform under 2 dyne/cm^2 while the Newtonian model has peak WSS concentrations throughout at over 4 dyne/cm^2.

Effect of Pediatric Hematocrit

Velocity fields between the three different physiological pediatric hematocrits (20, 40 and 60%) are compared at multiple points throughout the cardiac cycle with the modified GOB model. Figure 8 shows the velocity magnitude contours at peak systole. The general flow field is very similar between the three models with peak velocities increasing from 1.1 to 1.2 m/s in the ascending aorta and 1.31 to 1.36 m/s in the descending aorta (Fig. 8-A2). Additionally, velocity flow skews more toward the left subclavian artery (Fig. 8-D3) with increasing hematocrit. Flow in aortic arch and brachiocephalic and left common carotid arteries are nearly identical for all three hematocrits.

At mid-deceleration of systole, the comparisons are similar between the three hematocrits as at peak systole, however, the opposite trend in the descending aorta occurs (Figure 9). The velocity along the outer wall of the descending aorta decreases with increasing hematocrit from 1.03 m/s to 0.98 m/s (Fig. 9A-2, B-2). The other primary difference is an increase in velocity along the inner wall of the ascending aorta from 0.5 m/s at 20% hematocrit to 0.65 m/s at 60% hematocrit (Fig. 9-A1). There is also more flow into both the brachiocephalic and left common carotid arteries with increasing hematocrit while flow in the left subclavian artery remains constant.

At a later time point in the cardiac cycle, the onset of diastole, there are very significant differences in the velocity fields (Figure 10). The 20% hematocrit still has high velocity flow of 0.46 m/s into the aortic branches (Fig. 10-D) while the 40 and 60% hematocrits are 0.32 and 0.27 m/s, respectively. The 20% hematocrit also has higher velocities near the walls of

the ascending aorta (Fig. 10-A1, B1) but lower velocities in the descending aorta (Fig. 10-A2, B2) compared to the 40% and 60% hematocrits.

Figure 11 compares the WSS magnitudes between the three different pediatric hematocrits at three different points in the cardiac cycle. The regions of high WSS are similar between the three hematocrits at both peak systole and mid-deceleration of systole but vary in magnitude. Between the left common carotid and left subclavian artery branches maximum WSS values of 540 dynes/cm^2 are seen for the 20% hematocrit, 685 dynes/cm^2 for the 40% hematocrit, and 930 dynes/cm^2 for the 60% hematocrit at peak systole. At mid-deceleration of systole, peak WSS values are again seen between the left branches with values of 240, 310, and 420 dynes/cm^2 for the three hematocrits, respectively. Midway through diastole, however, the WSS's in the 20% hematocrit are higher throughout the aorta compared to the higher hematocrits. A maximum WSS of 6 dynes/cm^2 is seen on the proximal wall of the descending aorta in the 20% hematocrit compared to only 2 dynes/cm^2 in the 40 and 60% hematocrits.

Discussion

Both the flow field and the WSS in the pediatric aorta vary between the Newtonian and modified GOB pediatric blood models at different points in the cardiac cycle. Depending on the shear rates in the flow at a given point, the viscoelastic effects of the modified GOB model have varying degrees of effect. Figure 12-A shows that for shear rates less than 100 s^{-1} the viscosity of blood increases non-linearly with decreasing shear rate. However, at shear rates greater than 100 s^{-1} the viscosity is nearly constant and equal to the viscosity of the Newtonian model. Additionally, the viscoelastic effects are highly dependent on the blood hematocrit being modeled. For a 20% hematocrit the non-linear range of increasing viscosity is very small and occurs at shear rates less than 10 s^{-1}, making it nearly Newtonian. The 60% hematocrit model, however, has much stronger viscoelastic effects that will influence the flow even more at higher shear rates. Figure 12-B shows the volume of cells in the total pediatric aortic model that have shear rates less than 100 s^{-1} at different points previously investigated in the cardiac cycle. Comparing peak systole to mid-deceleration of systole and the onset of diastole, it is clear that a much lower total volume of cells is experiencing these low shear rates which lowers the impact of viscoelastic effects and makes the results closer to those of a Newtonian model. At later points in the cardiac cycle the inlet flow rate lessens and the shear rates begin to decrease throughout the aorta. As seen in figure 12-B, a much larger volume of cells in the aorta are experiencing lower wall shear rates, increasing the viscoelastic effect and leading to the more significant differences seen in both velocity and WSS between the Newtonian and modified GOB model and between each of the hematocrit models.

Flow Field

Both the Newtonian and GOB flows closely follows the contours of the aortic wall and are skewed towards the distal wall of the ascending aorta, inner wall of curvature in the aortic arch, and toward the proximal wall in the descending aorta (Fig. 6). These results compare well with the flow fields seen in previous experimental[20] and CFD work[34] in adult aortic

models that used a Newtonian assumption. The GOB flow, in contrast at the onset of diastole (Fig. 6), moves more coherently through the aortic arch leading to lower velocity flow reaching the branch arteries and higher velocity flow along the distal wall of the descending aorta. Previous work on flow in curved tubes has shown that if the flow is not developed prior to entering the curvature, the tube can act like a vortex and skew the velocity toward the inner wall. If the flow is fully developed upstream of the curve then the velocity can skew toward the outer wall[23]. In this model the short length of the ascending aorta does not allow for the flow to fully develop before entering the curvature of the aortic arch and therefore explains the skewed flow towards the outer wall of the arch and aortic branches.

While little previous work has been completed on non-Newtonian flow in the aorta, comparisons between other geometric models show similar trends in the flow profiles. Gijsen *et al.* studied the influence of non-Newtonian properties in a carotid bifurcation model under steady flow and in a 90° curved tube under pulsatile conditions[14,15]. They found in the carotid model that the shift in peak axial velocity towards the divider wall was less pronounced with the non-Newtonian fluid. In the 90° curve model they found slower development of secondary flows for the non-Newtonian fluid that heavily influenced the axial velocity profiles. Similarly, studies of blood flow through an arterial stenosis showed that non-Newtonian effects significantly weakened the distortion of flow patterns[27,36]. The hematocrit comparisons in this study most closely relate to these findings as increasing the hematocrit can be seen as moving from a more Newtonian fluid to a more non-Newtonian or viscoelastic fluid. Similar to Gijsen *et al.*, following the bifurcations into the aortic branches at the onset of diastole, the more non-Newtonian 60% hematocrit has a less pronounced skewness towards the vessel walls compared to the more Newtonian 20% hematocrit (Fig. 10D). Furthermore, flow in the descending aorta is more coherent following the aortic arch curvature in the 60% hematocrit compared to the more Newtonian 20% hematocrit (Fig. 10-A2, B2).

WSS

Overall, WSS varies throughout the entire aortic model depending on the blood model used, time point in the cardiac cycle, and the hematocrit. These WSS differences are much more significant than the velocity field differences and could have a greater impact on WSS dependent phenomena such as hemolysis and platelet activation and adhesion. Differences between the Newtonian and GOB model are seen at each time point in the cardiac cycle but are most important in later stages where the shear rates are lower than 100 s^{-1}. At peak systole, WSS is higher throughout the aorta with the GOB model compared to the Newtonian model. The locations of peak WSS are similar between the two models but vary in magnitude. Due to the similarity of the viscosity curves between the Newtonian and GOB models at these shear rates, minimal differences should be expected.

The areas of high WSS seen in this study compare well with previous work on pulsatile flow in an aortic model[12]. While Gao *et al.* neglected the aortic branches in their model, they still saw peak WSS values at the entrance to the ascending aorta and at the distal end of the aortic arch. Comparing WSS between Newtonian and non-Newtonian fluids, previous work has shown that non-Newtonian WSS in an adult aortic model is 10% higher in most places and

up to 40% higher at peak locations[23]. While the differences in this study were not as dramatic during systole there were still increases of 3–6% in WSS values throughout the GOB model (Fig. 7). In contrast to Gao *et al.*, the results during diastole for the GOB model predicted peak WSS values nearly half the magnitude of the Newtonian model. Studies of non-Newtonian versus Newtonian models in coronary arteries by Johnston *et al.* quantified the differences in WSS seen between the two models with a non-Newtonian importance factor[18]. There results showed that the non-Newtonian importance factor was much higher at lower center-line velocities and in regions of curvature in the artery. Both of these findings are similarly seen in this study, where at lower center-line velocities at later cardiac cycle time points the differences in WSS are much greater and thus the viscoelastic effect is more important. Additionally, the greatest differences seen in WSS peaks were also observed at highly curved regions of the model (the aortic branch bifurcations and at the distal end of the aortic arch into the descending aorta).

As discussed by Long *et al.* and seen in the results of this study, there is a strong viscoelastic dependence on patient hematocrit that significantly affects the hemodynamics and should be taken into consideration when developing pediatric blood analogs for experimental work or modeling pediatric blood in CFD[24].

Limitations

This study uses a pediatric aortic model based on detailed anatomical data. All dimensions are validated with existing morphological measurements by Machii and Becker[25] but both the diameters and lengths of different segments of the pediatric aorta can vary significantly between patients. Additionally, the model used is of a generalized pediatric aorta with a healthy aortic inflow. To better improve the design of PVADs, diseased state and surgically repaired aortic models should be studied in the future with the GOB model. Another limitation of this work is the lack of upstream modeling of blood flow out of the left ventricle and the effects of the aortic sinuses. A plug flow inlet velocity has been used to represent blood entering the ascending aorta while a true model of the upstream geometry would give more accurate inlet conditions.

Conclusion

This study is the first to examine pediatric hemodynamics using a viscoelastic model designed specifically for pediatric human blood. The results show the importance of using an accurate viscoelastic blood model instead of a Newtonian model, as the wide range in shear rates seen in the aorta throughout the cardiac cycle give rise to changes in the effective viscosity of blood. Moderate differences are seen in both the velocity fields and WSS during systole between a Newtonian and viscoelastic GOB model. However, significant differences are seen during diastole where the lower shear rates give rise to changes in viscosity and a greater influence of viscoelastic effects. Additionally, the wide variability in physiological pediatric hematocrit and the significant affect hematocrit has on pediatric aortic hemodynamics must be taken into consideration when performing any experimental or computational study.

Acknowledgments

We would like to acknowledge the National Institutes of Health for their support of this project through NIH NHLBI HL108123. Bryan C Good, Steven Deutsch, and Keefe B. Manning declare that they have no conflict of interest. No human or animal studies were carried out by the authors for this article. We also thank Ajit Yoganathan, PhD and Christopher M. Haggerty, PhD from the Department of Biomedical Engineering at the Georgia Institute of Technology for providing the pediatric aortic model.

References

1. Almond C, Morales D, Blackstone E, Turrentine M, Imamura M, Massicotte M, Jordan L, et al. Berlin heart excor pediatric ventricular assist device for bridge to heart transplantation in us children. Circulation. 2013; 127(16)
2. Anand M, Rajagopal K. A shear-thinning viscoelastic fluid model for describing the flow of blood. International Journal of Cardiovascular Medicine and Science. 2004; 4(2)
3. Bachmann C, Hugo G, Rosenberg G, Deutsch S, Fontaine A, Tarbell J. Fluid dynamics of a pediatric ventricular assist device. Artif Organs. 2000; 24(5)
4. Baldwin J, Borovetz H, Duncan B. The national heart, lung, and blood institute pediatric circulatory support program. Circulation. 2006; 113(1)
5. Canter C, Shaddy R, Bernstein D. Indications for heart transplantation in pediatric heart disease: a scientific statement from the american heart association council on cardiovascular disease in the young; the councils on clinical cardiology, cardiovascular nursing, and cardiovascular surgery and anesthesia: and the quality of care and outcomes research interdisciplinary working group. Circulation. 2007; 115(5)
6. Chandran KB. Flow dynamics in the human aorta. J Biomech Eng. 1993; 115(4B)
7. Chien S, Usami S, Dellenback R, Gregersen M. Blood viscosity: influence of erythrocyte deformation. Science. 1967:157.
8. Chien S, Usami S, Dellenback R, Gregersen M, Nanninga L, Guest M. Blood viscosity: influence of erythrocyte aggregation. Science. 1967:157.
9. Deville, O.; Gatski, T. Mathematical modeling for complex fluids and flows. Springer Science & Business Media; 2012.
10. Favero J, Secchi A, Cardozo N, Jasak H. Viscoelastic flow analysis using the software OpenFOAM and differential constitutive equations. J Non-Newton Fluid. 2010; 165(23–24)
11. Fogel M, Weinberg P, Rychik J, Hubbard A, Jacobs M, Spray T, Haselgrove J. Caval contribution to flow in the branch pulmonary arteries of fontan patients with a novel application of magnetic resonance presaturation pulse. Circulation. 1999; 99(9)
12. Gao F, Watanabe M, Matsuzawa T. Stress analysis in a layered aortic arch model under pulsatil blood flow. Biomed Eng Online. 2006; 5(25)
13. Giesekus H. A simple constitutive equation for polymer fluids based on the concept of deformation-dependant tensorial mobility. J Non-Newton Fluid. 1982; 11(1)
14. Gijsen F, van de Vosse F, Janssen J. The influence of the non-newtonian properties of blood on the flow in large arteries: unsteady flow in a 90 degree curved tube. J Biomech. 1999; 32(7)
15. Gijsen F, van de Vosse F, Janssen J. The influence of the non-newtonian properties of blood on the flow in larger arteries: steady flow in a carotid bifurcation model. J Biomech. 1999; 32(6)
16. Hakim S, Morshedian J, Narenji M, Nia P. Rheological Modelling of Caspian Pony Blood. Iranian Polymer Journal. 2001; 10(5)
17. Issa R. Solution of the implicitly discretised fluid flow equations by operator-splitting. J Comput Phys. 1986:62.
18. Johnston B, Johnston P, Corney S, Kilpatrick D. Non-Newtonian blood flow in human right coronary arteries: steady state simulations. J Biomech. 2004; 37(5)
19. Kent A, Kecskes Z, Shadbolt B, Falk M. Blood pressure in the first year of life in healthy infants born at term. Pediatr Nephrol. 2007; 22(10)
20. Ku D. Blood flow in arteries. Annu Rev Fluid Mech. 1997; 29(1)

21. Leonov A. Nonequilibrium thermodynamics and rheology of viscoelastic polymer media. Rheologica acta. 1976; 15(2)
22. Linderkamp O, Versmold H, Riegel K, Betke K. Contributions of red cells and plasma to blood viscosity in preterm and full-term infants and adults. Pediatrics. 1984; 74(1)
23. Liu X, Fan Y, Deng X, Zhan F. Effect of non-newtonian and pulsatile blood flow on mass transport in the human aorta. J Biomech. 2011; 44(6)
24. Long J, Undar A, Manning K, Deutsch S. Viscoelasticity of pediatric blood and its implications for the testing of a pulsatile pediatric blood pump. ASAIO J. 2005; 51(5)
25. Machii M, Becker A. Morphologic features of the normal aortic arch in neonates, infants, and children pertinent to growth. Ann Thorac Surg. 1997; 64(2)
26. Mah D, Singh T, Thiagarajan R, Gauvreau K, Piercey G, Blume E, Fynn-Thompson F, Almond C. Incidence and risk factors for mortality in infants awaiting heart transplantation in the USA. J Heart Lung Transpl. 2009; 28(12)
27. Nakamura M, Sawada T. Numerical study on the flow of a non-newtonian fluid through an axisymmetric stenosis. J Biomech Eng. 1988; 110(2)
28. Pantalos G, Giridharan G, Colyer J, Mitchel M, Speakman J, Lucci C, Johnson G, Gartner M, Koenig S. Effect of continuous and pulsatile left ventricular assist on pulsatility in a pediatric animal model of left ventricular dysfunction: pilot observations. ASAIO J. 2007; 53(3)
29. Pekkan K, Dur O, Sundareswaran K, Kanter K, Fogel M, Yoganathan A, Undar A. Neonatal aortic arch hemodynamics and perfusion during cardiopulmonary bypass. J Biomech Eng. 2008; 130(6)
30. Pekkan K, Frakes D, De Zelicourt D, Lucas C, Parks J, Yoganathan A. Coupling pediatric ventricle assist devices to the fontan circulation: simulations with a lumped-parameter model. ASAIO J. 2005; 51(5)
31. Phillips W, Deutsch S. Towards a constitutive equation for blood. Biorheology. 1975; 12(6)
32. Rajagopal K, Srinivasa A. A thermodynamic framework for rate-type fluid models. J Non-Newton Fluid. 2000; 88(3)
33. Reinhart W, Danoff S, King R, Chien S. Rheology of fetal and maternal blood. Pediatr Res. 1985; 19(1)
34. Shahcheraghi N, Dwyer H, Cheer A, Barakat I, Rutaganira T. Unsteady and three-dimensional simulation of blood flow in the human aortic arch. J Biomech Eng. 2002; 124(4)
35. Thurston G. Viscoelasticity of human blood. Biophys J. 1972; 12(9)
36. Tu C, Deville M. Pulsatile flow of non-newtonian fluids through arterial stenoses. J Biomech. 1996; 29(7)
37. Yang N, Deutsch S, Paterson E, Manning K. Numerical study of blood flow at the end-to-side anastomosis of a left ventricular assist device for adult patients. J Biomech Eng. 2009; 131(11)
38. Yang N, Deutsch S, Paterson E, Manning K. Comparative study of continuous and pulsatile left ventricular assist devices on hemodynamics of a pediatric end-to-side anastomotic graft. Cardiovasc Eng Technol. 2010; 1(1)
39. Yang N, Deutsch S, Paterson E, Manning K. Hemodynamics of an end-to-side anastomotic graft for a pulsatile pediatric ventricular assist device. J Biomech Eng. 2010; 132(3)
40. Yeleswarapu, K. PhD Dissertation. Pittsburgh, PA: 1996. Evaluation of continuum models for characterizing the constitutive behavior of blood.

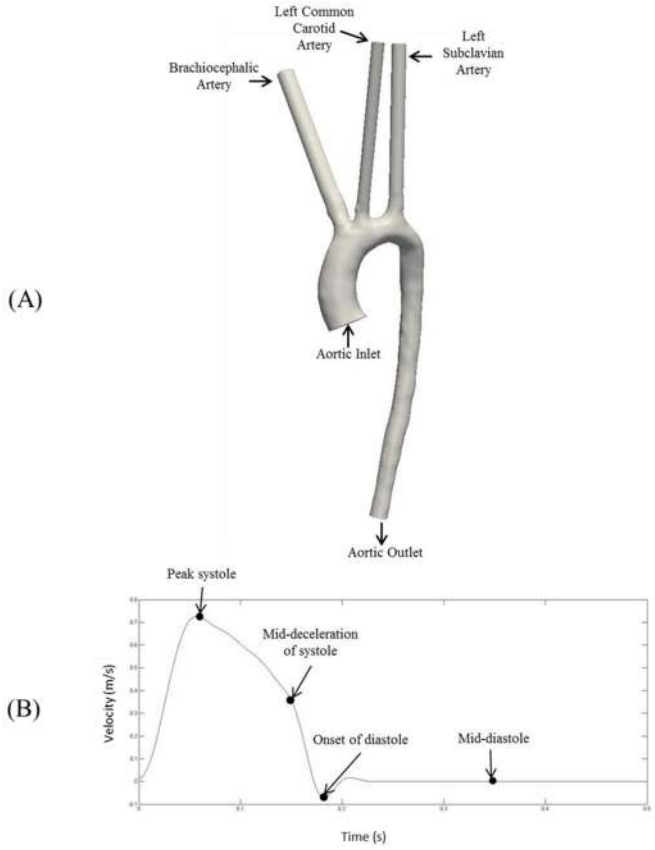

Figure 1.

A) Generalized pediatric aorta model (NIH-Georgia Tech Fontan Anatomy Database ID: CHOP007) scaled to represent a one year old patient. B) Scaled velocity waveform (26) to represent a healthy pediatric patient with cardiac output of 1 L/min and heart rate of 120 bpm. Four time points of the cardiac cycle (peak systole, mid-deceleration of systole, onset of diastole, and mid-diastole) are analyzed.

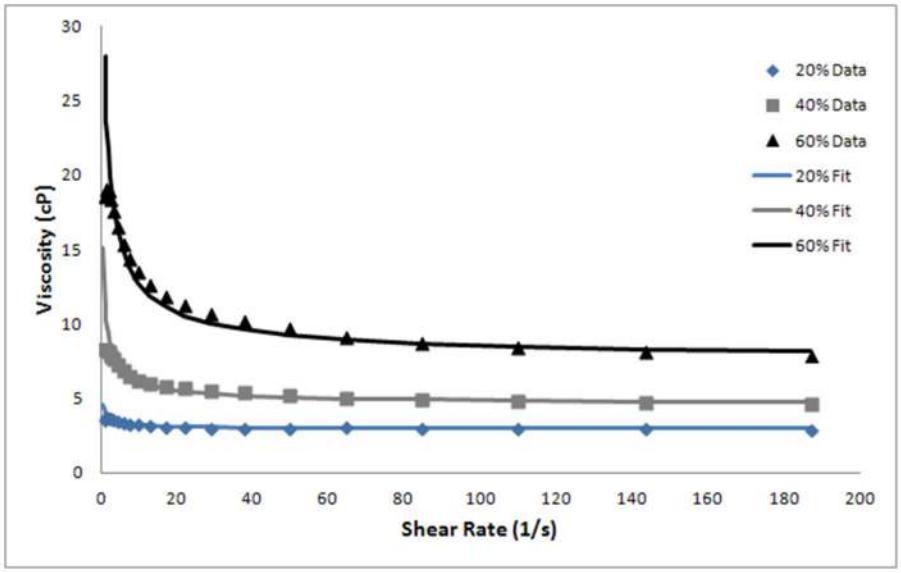

Figure 2.
Viscosity versus shear rate data for pediatric blood hematocrits of 20, 40 and 60%[24] with their corresponding modified GOB model fits.

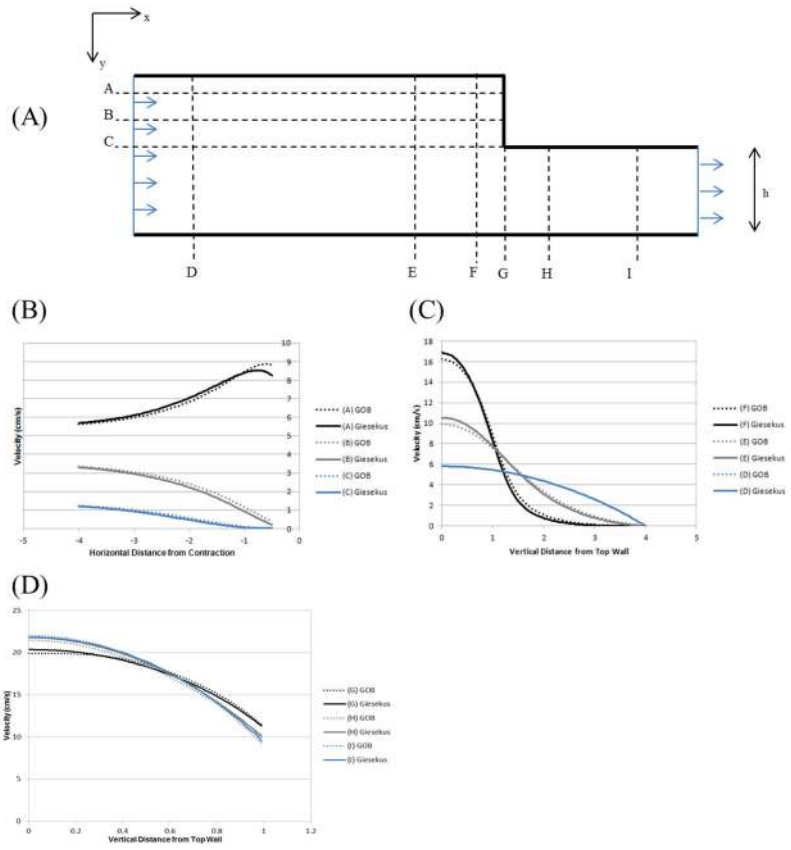

Figure 3.

A) 4:1 contraction model used to validate GOB solver against previously validated Giesekus[13] model fitted to the same experimental data with viscoelasticFluidFoam[10]. Upstream horizontal velocity profiles (cm/s) are normalized to the contraction length (B), while vertical velocity profiles are normalized to the contraction height (h) at upstream (C) and downstream (D) locations.

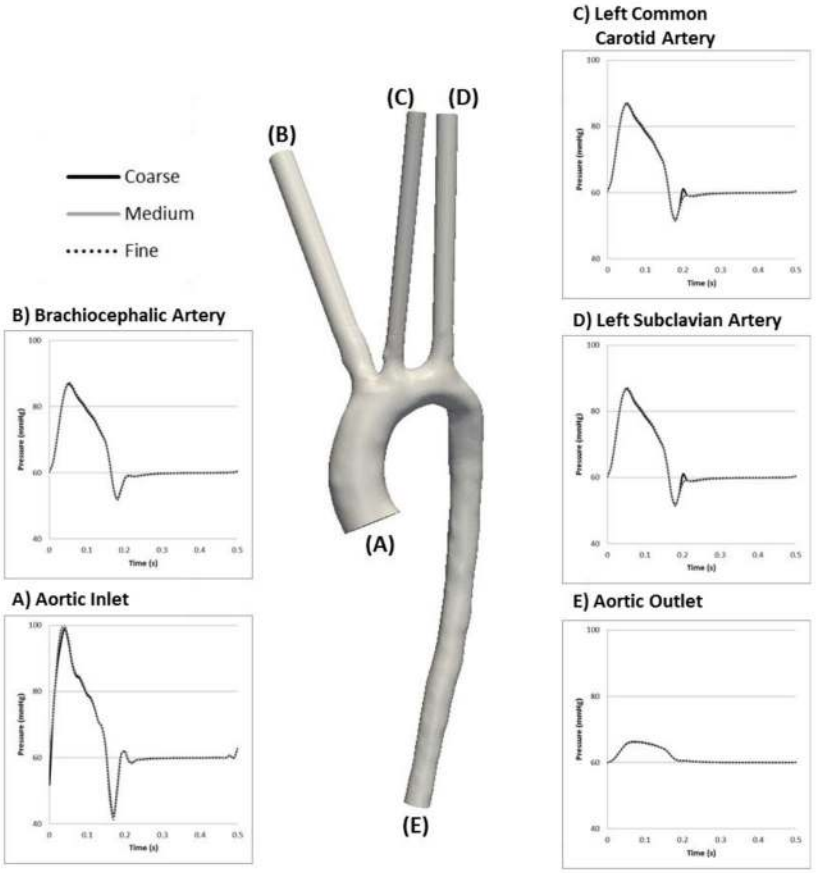

Figure 4.

Integrated inlet and outlet pressures (mmHg) for three grids (coarse, medium and fine) over a single cardiac cycle.

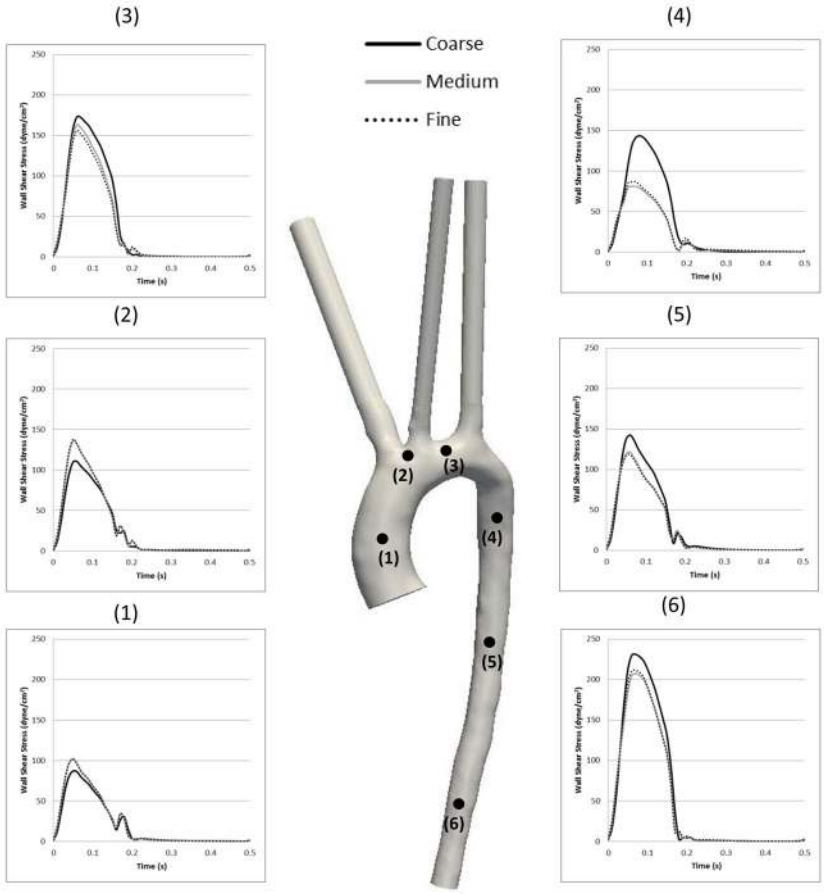

Figure 5.

WSS magnitudes (dyne/cm^2) at six locations along the length of the aorta for three grids (coarse, medium and fine) over a single cardiac cycle.

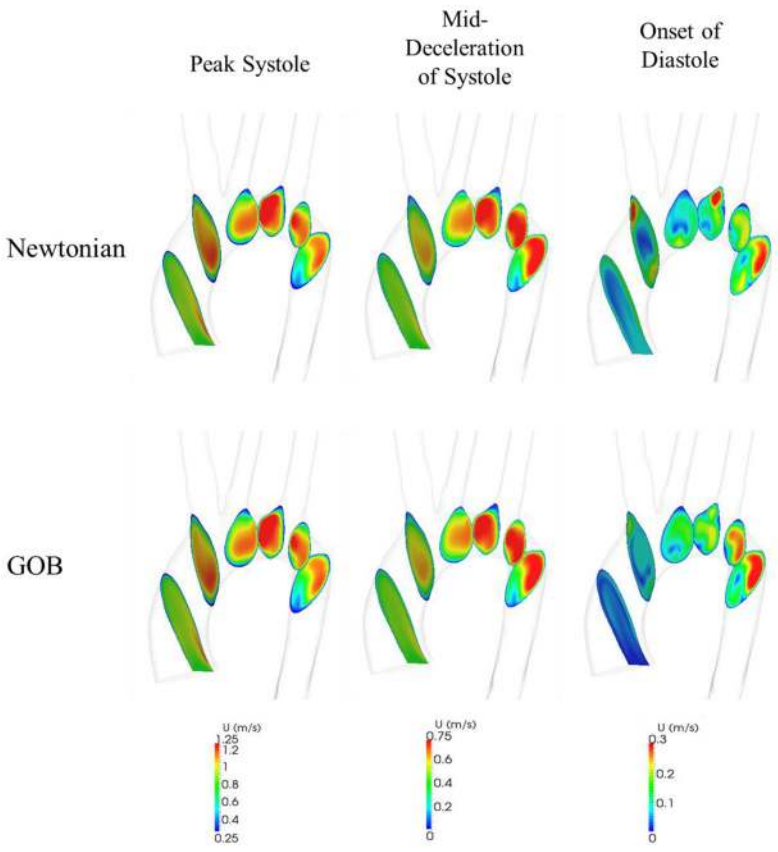

Figure 6.

Velocity magnitude contour (m/s) comparison between 60% hematocrit Newtonian and GOB models at three points in the cardiac cycle (peak systole, mid-deceleration of systole, and onset of diastole). Note the different velocity scales at each time point.

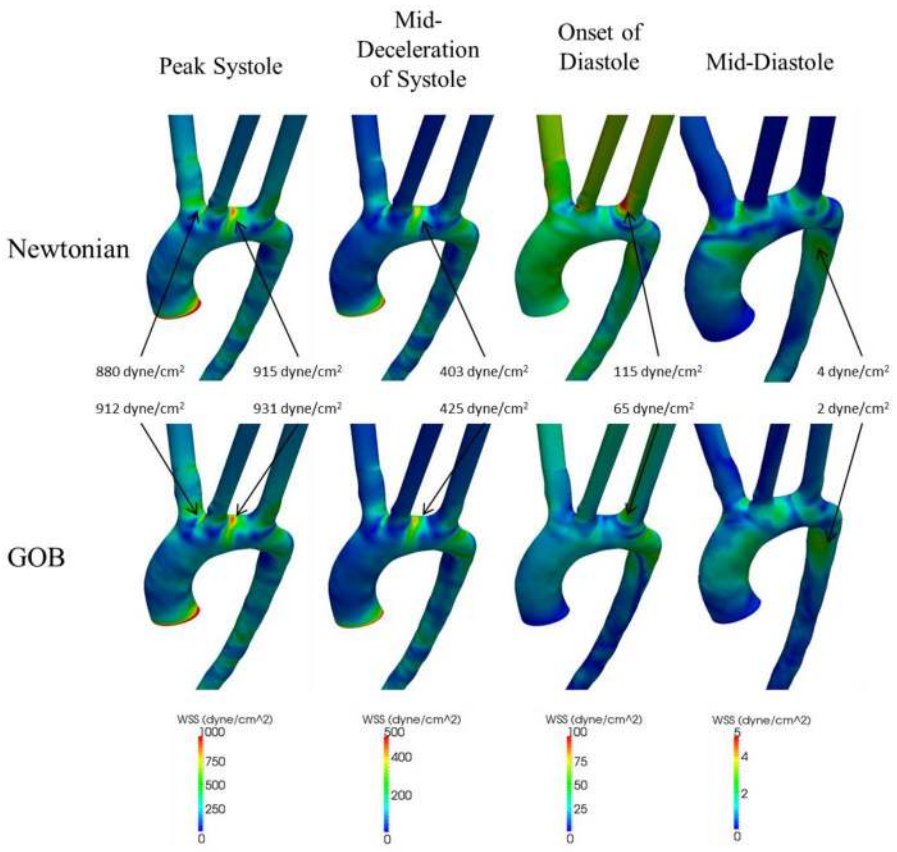

Figure 7.

WSS magnitude contour (dynes/cm^2) comparison between 60% hematocrit Newtonian and GOB models at four points in the cardiac cycle (peak systole, mi-deceleration of systole and onset of diastole). Note the different WSS scales at each time point.

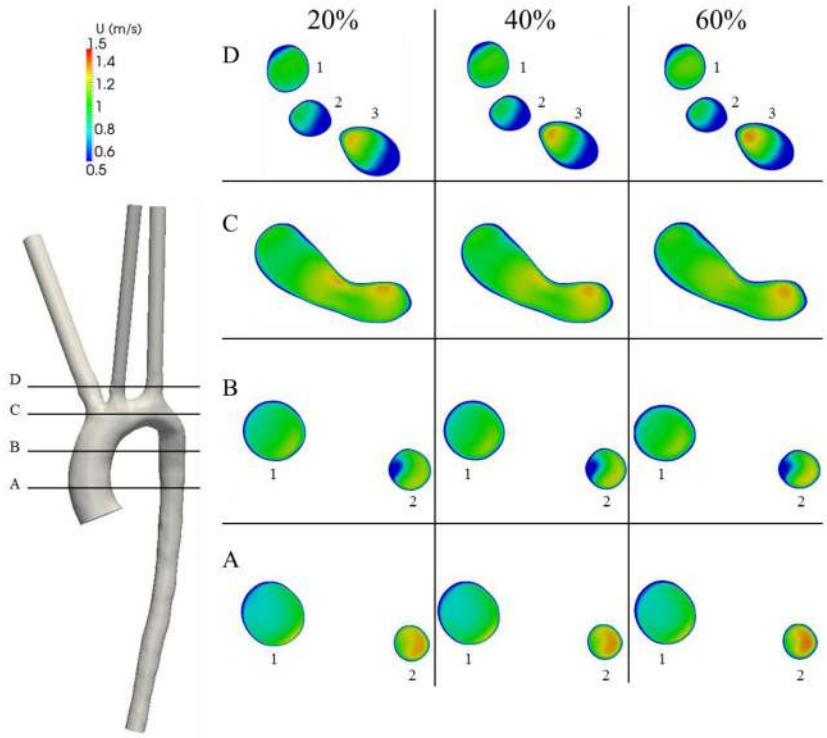

Figure 8.
Velocity magnitude contour (m/s) comparison between 20, 40, and 60% hematocrit GOB models at peak systole.

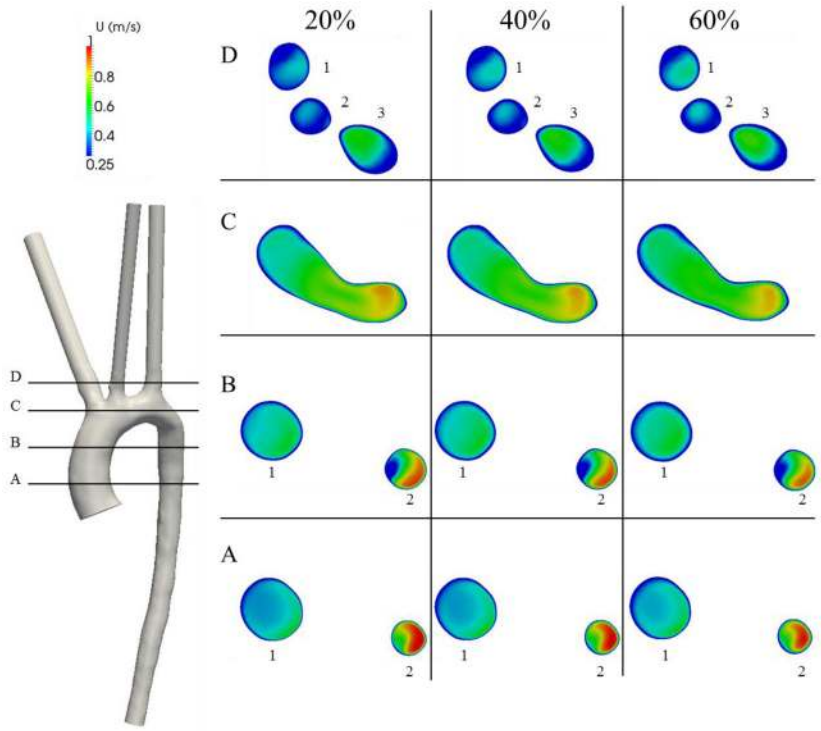

Figure 9.

Velocity magnitude contour (m/s) comparison between 20, 40, and 60% hematocrit GOB models at mid-deceleration of systole.

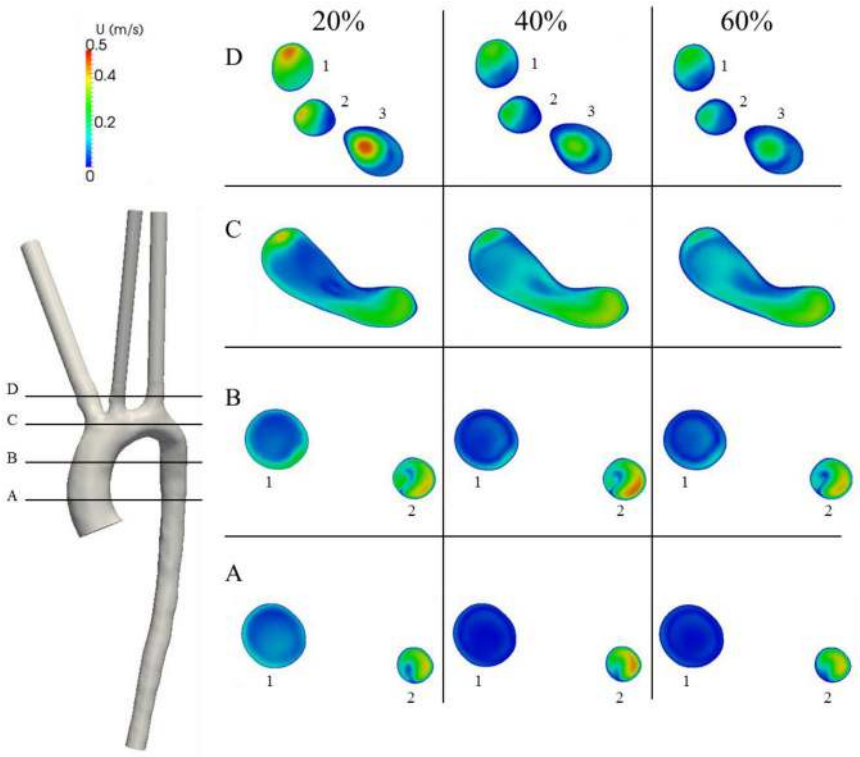

Figure 10.
Velocity magnitude contour (m/s) comparison between 20, 40, and 60% hematocrit GOB models at the onset of diastole.

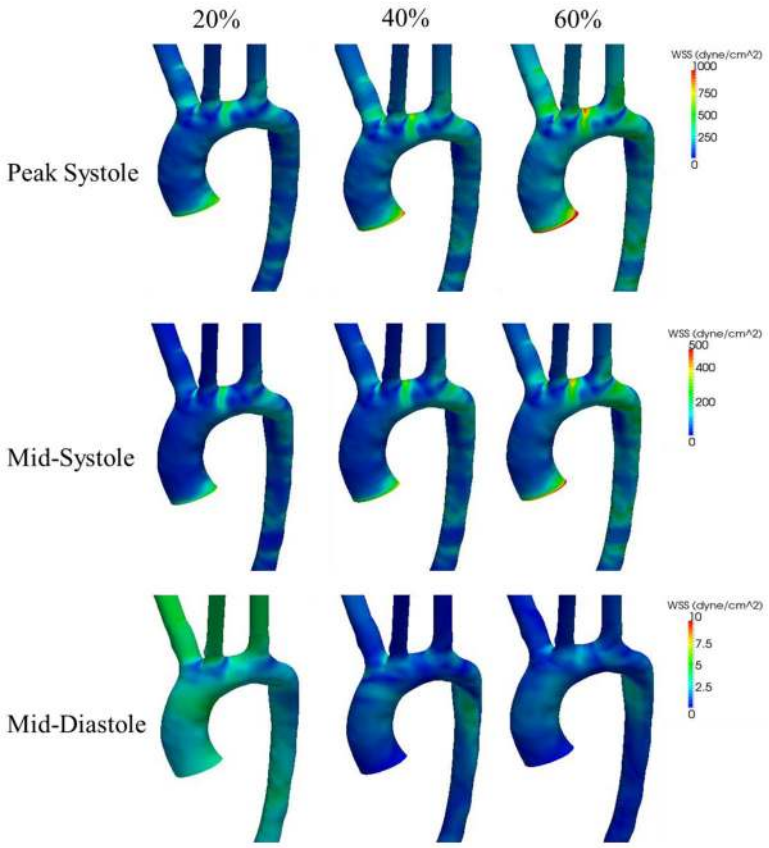

Figure 11.

WSS magnitude contour (dynes/cm^2) comparison between 20, 40, and 60% hematocrit GOB models at three points in the cardiac cycle (peak systole, mid-deceleration of systole and mid-diastole). Note the different WSS scales at each time point.

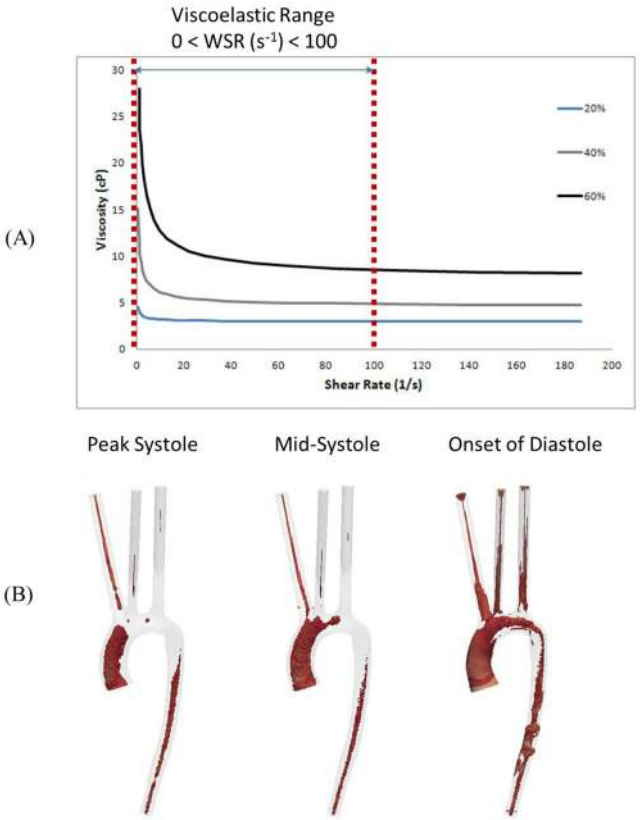

Figure 12.

A) Range of shear rates where the viscoelastic effects of the three different hematocrit GOB models are important. B) Volume of computational cells experiencing wall shear rates in the important viscoelastic range at three different points in the cardiac cycle (peak systole, mid-deceleration of systole, and onset of diastole).

Table 1

Modified GOB Coefficients from Viscosity Model Fit

Hematocrit (%)	η(cP)	η_l (cP)	μ(cP/s)
20	4.2	5.8	1.1
40	31.1	8.9	5.3
60	45.2	14.8	19.8